Article

Ab Initio Double-Differential Ionization Cross-Section Calculations in Antiproton–Helium Collisions

Imre Ferenc Barna [1,*], Mihály András Pocsai [1] and Károly Tőkési [2]

1 Wigner Research Centre for Physics, Konkoly-Thege Miklós út 29-33, H-1121 Budapest, Hungary
2 Institute for Nuclear Research (ATOMKI), H-4026 Debrecen, Hungary
* Correspondence: barna.imre@wigner.hu

Abstract: We present ionization cross-sections for antiproton and helium collisions based on an ab initio time-dependent coupled channel method. In our calculations, a finite basis set of regular helium Coulomb wave packets and Slater function were used. The semiclassical approximation was applied with the time-dependent Coulomb potential to describe the antiproton–electron interaction. Three different projectile energies were considered as 10, 50 and 100 keV. We found clear evidence for the formation of the anti-cusp in the differential distributions.

Keywords: ab initio time-dependent coupled channel method; ionization; antiproton; anti-cusp

1. Introduction

The collision between antiprotons and atoms is of fundamental interest in atomic physics. In the 1990s, numerous experimental and theoretical works were performed with low-energy antiprotons, investigating various interesting phenomena [1]. Protons and antiprotons are the lightest heavy ions, where the semiclassical approximation is valid, and their motion can therefore be classically treated. In contrast to proton–antiproton collisions—due to the negative charge—no electron transfer can take place, which makes the electron dynamics much simpler at low energies.

In theoretical multi-electron atomic physics, the investigation of antiproton–helium collision is of crucial interest.

There have been three benchmark experiments wherein the total cross-ionization sections were measured for low-energy collisions between the antiprotons and helium atoms. The first two measurements were performed in 1990 [2] and 1994 [3]. Subsequently, the single- and double-ionization cross-sections of the He and Ar atoms were investigated [4] by antiproton impact.

These experiments induced the "competition" between the theories for the increasingly improving descriptions of the physical processes, which are still very much active. In general, all theoretical descriptions predict almost similar results above 100 keV in antiproton collision energy due to the weakening Sommerfeld parameter. This means that the interaction becomes perturbative and the first Born approximation is valid. The deviation between theory and experimental data becomes clearly visible between impact energies of 10 and 100 keV and below a projectile energy of 10 keV, there are large deviations between non-perturbative ab initio calculations. This is a clear indicator that the role of electron–electron correlation is crucial. However, until now, there has been no clear evidence of which theoretical model is superior.

This paper now starts with a brief and non-exhaustive historical overview of the relevant theoretical models. The forced impulse method (FIM), developed by Reading and Ford [5], was one of the most successfully early methods for proton–antiproton and antiproton–helium collisions. An improved version of FIM is the multi-cut forced impulse (MFIM) method by [6]. Bent et al. [7] used multi-electron hidden crossing (MEHC) theory

in their study of the single ionization of He in the impact between antiproton and helium. The time-dependent density functional theory [8] is another powerful method to describe non-perturbative many-electron ionization processes, even in the low keV/amu impact energy range. Keim et al. [9] applied density functional theory with various response functions and with a basis representation obtained from the basis generator method (BGM) to obtain single- and double-ionization cross-sections in antiproton and helium collision systems. Later, the method was improved and the same scientific question was subsequently revised [10]. The single ionization of He–antiproton impact was also studied by Tong et al. [11] using a self-interaction-free time-dependent density-functional theory (SIF-TDDFT).

Various independent particle close-coupling methods in a semi-classical impact parameter treatment—wherein the electron wave function is expanded around the target nucleus—are prominent among the theoretical studies [12–17].

Later, a fully correlated, three-dimensional approach was developed by Schulz and Krstic [18] to study the ionization cross-sections in collisions between antiproton and helium atoms. They solved the time-dependent Schrödinger equation (TDSE) in a four-dimensional Cartesian lattice (LTDSE) and calculated the ionization cross-sections using 75^4 lattice points. The B-spline basis for the construction of the active electron wave function was used by Sahoo et al. [19]. B-splines have been widely used in atomic physics [20] because of their ability to accurately represent the continuum channels when compared with other conventional bases. Foster [21] published calculations obtained from a lattice time-dependent close coupling method.

Fainstein et al. [22] applied the Coulomb-distorted wave Eikonal initial state (CDW-EIS) method below 100 keV antiproton impact energies and had an astonishingly good agreement with the experimental data of [3]. This induced a debate regarding the validity of CDW-EIS method.

The independent particle approach was also performed by Schultz [23] using a classical trajectory Monte Carlo Method (CTMC).

First, we applied a time-dependent coupled channel (TDCC) method on a special basis for calculating the single ionization cross-sections. Our results for angular differential ionization cross-sections were compared with the results of CDW-EIS and CTMC methods [24]. Later, the energy and angular differential electron emission cross-sections were also presented using the CDW-EIS and CTMC models [25].

In 2011, Kirchner and Knudsen published a topical review which exhaustively discussed and compared all the experimental results and theoretical model calculations [26]. In recent years, numerous additional studies were published regarding antiproton–helium or antiproton–atom and antiproton–molecule collisions from basically the same groups [27–34].

In parallel to the development of theoretical ab initio methods, there must also be a focus on the deeper understanding of the dynamics of the anti-cusp dip, where DDCSs must be analyzed.

An interesting subject in collision physics is the study of electron emissions in the direction of projectile motion. The electron capture-to-continuum (ECC) peak was discovered in 1970 by [35] in the double-differential cross-section (DDCS) of electrons ejected in proton–atom collisions at 0 degrees compared to the projectile's initial velocity.

For positively charged particles, the production of the cusp peak is experimentally and theoretically understood [36]. Numerous investigations lead to the conclusion that the cusp is generated when the asymptotic velocity of the ionized electron is equal to the velocity of the projectile.

It can be explained, for positively charged projectiles, as a result of the special case of ionization, where the ionized target electron is strongly influenced by the outgoing projectile, or in other words, when the atomic electron is dragged by the projectile continuum state and moves with it. Following this scenario, using the negatively charged projectiles, we can expect an electron yield deficit in the direction of the projectile path and we can expect anti-cusp formation instead of cusp formation.

However, for a negatively charged projectile impact, due to the very limited availability of experimental data, the production of the anti-cusp is barely understood, especially at low-impact energies. The anti-cusp supposes that a well-defined gap must exist in the energy spectrum of the ionized electron in the direction of the projectile. Numerous theoretical studies from different authors have addressed the question of the anti-cusp [37–42]. To the best of our knowledge, only the total ionization cross-section data have been made available from experiments to date and there are no available *ab initio* calculations for the differential ionization cross-sections for the impact of an antiproton–helium collision.

In this work, we present ionization cross-sections for antiproton–helium collisions based on an *ab initio* time-dependent coupled channel method. In our calculations, a finite basis set of regular helium Coulomb wave packets and Slater functions were used. We show the results for singly and doubly differential cross-sections at antiproton impact energies of 10, 50 and 100 keV. Thus, we believe that this study might stimulate experimentalists to investigate this problem in low-energy antiproton–atom collisions in the future.

This paper contains a brief outline the theoretical approach used (Section 2) whilst the calculated results are presented and discussed in Section 3. Atomic units are used throughout the paper unless otherwise indicated.

2. Theory

The TDCC method has been widely used in various fields of atomic collision physics with the recognition that it is one of the most reliable and powerful theoretical approaches [26]. Our single-center coupled-channel method was first introduced for the ionization of helium in relativistic heavy-ion collisions [43,44]. Later, the same model was applied for positron helium collisions [45]; for photoionization [46], and finally, for the two-photon double-ionization of helium [47]. Currently, a very similar model was used to investigate the photoionization of rubidium atoms [48].

In the semi-classical approximation, the projectile moves in a straight-line trajectory, with constant velocity v and impact parameter b. The projectiles are considered to be classical point charges without any inner structure.

To study the ionization process, the time-dependent Schrödinger equation is solved with a time-dependent external Coulomb field:

$$i\frac{\partial}{\partial t}\Psi(\mathbf{r}_1, \mathbf{r}_2, t) = \left(\hat{H}_{He} + \hat{V}(t)\right)\Psi(\mathbf{r}_1, \mathbf{r}_2, t),$$ (1)

where $\hat{H}_{He}$ is the Hamiltonian of the unperturbed helium atom

$$\hat{H}_{He} = \frac{p_1^2}{2} + \frac{p_2^2}{2} - \frac{2}{r_1} - \frac{2}{r_2} + \frac{1}{|\mathbf{r}_1 - \mathbf{r}_2|}.$$ (2)

To describe the antiproton–electron interaction $\hat{V}(t)$, the time-dependent Coulomb potential is used:

$$\hat{V}(t) = \left(\frac{1}{R_1(t)} + \frac{1}{R_2(t)}\right)$$ (3)

with $R_i(t) = ((x_i - b)^2 + y_i^2 + (z_i - v_p t)^2)^{1/2}, i = 1, 2$. Below 20 keV, impact energies were used instead of the straight-line trajectories of Coulomb hyperbolas and the well-known deflection angle formula was applied for the outgoing antiproton particle [49]. For collision energies below 1 keV, the trajectory bending effect is even more important. Equation (1) is solved by the expansion of $\Psi(\mathbf{r}_1, \mathbf{r}_2)$ on the basis of eigenfunctions $\{\Phi_j\}$ of the time-independent Schrödinger equation:

$$\hat{H}_{He}\Phi_j(\mathbf{r}_1, \mathbf{r}_2) = E_j\Phi_j(\mathbf{r}_1, \mathbf{r}_2),$$ (4)

with

$$\Psi(\mathbf{r}_1, \mathbf{r}_2, t) = \sum_{j=1}^{N} a_j(t)\Phi_j(\mathbf{r}_1, \mathbf{r}_2)e^{-iE_j t}, \tag{5}$$

where $a_j(t)$ are the time-dependent expansion coefficients for the various channels described by the wave functions Φ_j. Inserting this Ansatz into Equation (1) leads to a system of first-order differential equations for the expansion coefficients:

$$\frac{da_k(t)}{dt} = -i \sum_{j=1}^{N} V_{kj}(t)a_j(t)e^{i(E_k - E_j)t}, \quad (k = 1, \dots, N), \tag{6}$$

where V_{kj} is the coupling matrix $\langle \Phi_k(\mathbf{r}_1, \mathbf{r}_2)|\hat{V}(t)|\Phi_j(\mathbf{r}_1, \mathbf{r}_2)\rangle$ including the symmetrized products of the projectile–electron single-particle interaction matrix elements and electron–electron single-particle overlap matrix elements, respectively.

Denoting the ground state with $k = 1$, the following initial conditions are used

$$a_k(t \to -\infty) = \begin{cases} 1 & \text{for } k = 1, \\ 0 & \text{for } k \neq 1. \end{cases} \tag{7}$$

The total cross-section for occupying the helium eigenstate k can be calculated as an integral over the impact parameter $\mathbf{b}$

$$\sigma_k = \int P_k(\mathbf{b}, t \to \infty)d^2 b, \tag{8}$$

with the probability

$$P_k(\mathbf{b}, t \to \infty) = |a_k(t \to \infty)|^2. \tag{9}$$

The coupled system of Equation (6) is numerically solved using a fifth-order Runge–Kutta–Fehlberg method with embedded automatic time step regulation. The conservation of the norm of the wave function is fulfilled better than 10^{-8} during the collision.

The eigenfunctions Φ_j in Equation (4) are obtained by diagonalizing the Hamiltonian on the basis of orthogonal symmetrized two-particle functions f_μ so that

$$\Phi_j(\mathbf{r}_1, \mathbf{r}_2) = \sum_\mu b_\mu^{[j]} f_\mu(\mathbf{r}_1, \mathbf{r}_2). \tag{10}$$

In the applied independent particle model, the many-particle wave functions f_μ are built up from single-particle orbitals. For these single-particle wave functions, an angular momentum representation with spherical harmonics $Y_{l,m}$, hydrogen-like radial Slater functions and radial regular Coulomb wave packets is used. The Slater function can be written in the form of:

$$S_{n,l,m,\kappa}(\mathbf{r}) = c(n, \kappa)r^{n-1}e^{-\kappa r}Y_{l,m}(\theta, \varphi), \tag{11}$$

where $c(n, \kappa)$ is the normalization constant. A regular Coulomb wave packet

$$C_{k,l,m,Z}(\mathbf{r}) = q(k, \Delta k)Y_{l,m}(\theta, \varphi) \int_{E_k - \Delta E_k/2}^{E_k + \Delta E_k/2} F_{k,l,Z}(r) \, dk \tag{12}$$

with normalization constant $q(k, \Delta k)$ is constructed from the radial Coulomb function [50]

$$\begin{aligned} F_{k,l,Z}(r) = \ & \sqrt{\frac{2k}{\pi}}e^{\frac{\pi\eta}{2}}\frac{(2\rho)^l}{(2l+1)!}e^{-i\rho} \mid \Gamma(l+1-i\eta)\mid \times \\ & {}_1F_1(1+l+i\eta, 2l+2, 2i\rho), \end{aligned} \tag{13}$$

where $\eta = Z/k$, $\rho = kr$.

The wave packets cover a small energy interval ΔE_k and thereby form a discrete representation of the continuum which can be incorporated into the finite basis set. The normalized Coulomb wave packets are calculated up to a radial distance of more than 300 a.u. to achieve a deviation of less than one percent from unity in their norm.

In this approach, two different effective charges Z for the target nucleus were used to take into account the difference between the singular- and the double-ionized stats of the He atoms. For the single-ionized and double-ionized states, $Z = 1$ and $Z = 2$ were used, respectively.

The single- and double-continuum electron sates were equidistantly calculated up to an energy of 6 a.u.

We included single-particle wave functions with $0 \leq l_1, l_2 \leq 2$ angular momenta and coupled them to $0 \leq L \leq 2$ total angular momentum two-electron states. For the $L = 0$ configurations, we used ss+pp+dd angular correlated wave functions; for $L = 1$, we used sp+pd couplings; and for $L = 2$, we used the sd+pp+dd configurations. For the ground state energy of He (1s1s), the -2.901 a.u. was obtained which was reasonably accurate compared to the "exact" value of -2.903 a.u.

The diagonalization process gives 465 basic states which correspond to 1490 different collision channels, including different m_l sub-states. The highest energy eigenvalue lies at 27.8 a.u. Numerous different basis sets were applied in order to test for the convergence of the expansion (5). The results demonstrate that the channels with energies above 5 a.u contribute very little to the ionization probabilities. The basis between the first ionization threshold (-2.0 a.u.) and the lowest auto-ionizing quasi-bound state ("2s2s" E $= -0.77$ a.u. L $= 0$) contained 22 discretized continuum states per total angular momentum, providing the major contribution for single-ionization.

The Feshbach projection [43] together with complex scaling were adopted in order to separate excitation as well as double- and single-ionization cross-sections. In the first step, a new "reference" Hilbert subspace $\Psi(\mathbf{r}_1, \mathbf{r}_1)^r$ was constructed and split into three different orthogonal subspaces characterized by the properties of the two electrons: 1—bound–bound; 2—bound–ionized; and 3—ionized–ionized electrons. In the second step, our helium wave function Equation (10) was projected onto the reference space and this determined the excitation as well as the single- and double-ionization contributions. We may formally write this expansion as:

$$\Phi_j(\mathbf{r}_1, \mathbf{r}_2) = C_1 \Psi(\mathbf{r}_1, \mathbf{r}_1)_1 + C_2 \Psi(\mathbf{r}_1, \mathbf{r}_1)_2 + C_3 \Psi(\mathbf{r}_1, \mathbf{r}_1)_3 \tag{14}$$

where the left hand side is our helium wave function, and C_1, C_2 and C_3 are the expansion coefficients of the bound–bound, bound–ionized or double-ionized contributions in the form of

$$C_i = \langle \Psi(\mathbf{r_1}, \mathbf{r_1}) | \Phi_j(\mathbf{r}_1, \mathbf{r}_2) \rangle. \tag{15}$$

A detailed description can be found in our first publication [43]. To fix the effective charge of the Coulomb wave function used in the helium wave functions, the excitation and single-ionization cross-sections were compared with the results obtained from the complex scaling [46]. Doubly-excited states embedded in the continuum, e.g., "2s2s" (this labeling should not be taken literally because of the strong electron–electron correlation [51]), can be identified by the method of complex scaling and therefore the double-excitation and the single-ionization states can be separated. This new combination of the two methods is still not exactly rigorous but is much more feasible than the Feshbach method alone and therefore reduces ambiguity.

To calculate the angular-differential ionization cross-sections, the density operator was taken, which can be found in regular quantum mechanical textbooks [52]. The electron final-state density can be determined from the time-dependent wave function after the collision

$(t \to \infty)$ according to the expectation value of the density operator $\hat{\rho} = \sum_{i=1,2} \delta(\mathbf{r} - \mathbf{r}_i)$ for a fixed-impact parameter $\mathbf{b}$

$$\rho_{\mathbf{b}}(\mathbf{r}) = \left\langle \Psi(\mathbf{r}_1, \mathbf{r}_2) \left| \sum_{i=1,2} \delta(\mathbf{r} - \mathbf{r}_i) \right| \Psi(\mathbf{r}_1, \mathbf{r}_2) \right\rangle. \tag{16}$$

In order to extract the angular distribution of the ionized electrons, two additional operations are needed:

1. The wave function Ψ is projected onto the single-ionization continuum $|\Psi_{ion}\rangle = (1 - \hat{P}_b - \hat{P}_{di}) \, |\Psi\rangle$, where $\hat{P}_b$ is the projector onto the bound state subspace (including all excited states) and $\hat{P}_{di}$ is the projector onto double-ionized states. The corresponding formulas can be found in our former works [43,44].

2. The radial and the azimuthal coordinates have to be integrated to obtain the polar angle distribution of the ionized electrons:

$$P_{\mathbf{b}}(\theta) = \frac{1}{2\pi} \int_0^{2\pi} \int_0^{\infty} \langle \Psi_{ion} | \sum_{i=1,2} \delta(\mathbf{r} - \mathbf{r}_i) | \Psi_{ion} \rangle r^2 dr d\varphi =$$

$$\frac{1}{\pi} \int_0^{2\pi} \int_0^{\infty} \int_{\mathbf{r}_1} |\Psi_{ion}|^2 d^3 r_1 r^2 dr d\varphi. \tag{17}$$

The angular differential cross-section is obtained by integrating $P_{\mathbf{b}}(\theta)$ over the impact parameter. This method was already used in a previous publication [24] and it gives a satisfactory agreement with other theoretical results.

In contrast with other perturbative or classical approaches, TDCC methods has a finite number of discretized final-states. This is why it is not possible to calculate energy-differential cross-sections in a rigorous way—only the distribution of the channel cross-sections divided by an effective energy can be obtained. This effective energy can be defined in different ways, and it can be the energy of the corresponding channel; the difference in the energies of the two neighboring channels or the widths of the Coulomb wave packets (12). Here, we consider the last one, and we use the form for calculating the approximated energy differential cross-sections according to the following equation:

$$\frac{d\sigma}{dE} \approx \frac{\sigma_k}{\Delta E_k}. \tag{18}$$

3. Results and Discussions

Figure 1 shows our recent total single-ionization cross-sections in collisions between low-energy antiprotons and helium atoms with some of the latest theoretical data and with the three known experimental datasets. It is worth mentioning that, above an antiproton energy of 100 keV, all theoretical and experimental data run together, the interaction becomes increasingly weak and even perturbative methods work quite well. Between antiproton energies of 10 and 100 keV, the discrepancy between theory and experimental results grows. Below an energy of 10 keV, the newest experimental results run nicely together with the two presented theoretical calculations.

In the last three decades, numerous theoretical methods have been developed to calculate the total single ionization cross-sections in low-energy antiproton–helium collisions. It is obvious that we cannot present all the theoretical results on a single figure without confusion, so for a better overview, Figure 2 presents additional nine different theoretical curves and compared with each other. We can clearly see again that above 100 keV—in the perturbative region—all curves come together. Between 10 and 100 keV, the discrepancy enhances. Below 10 keV—where the field of the projectile is very strong—results diverge from each other.
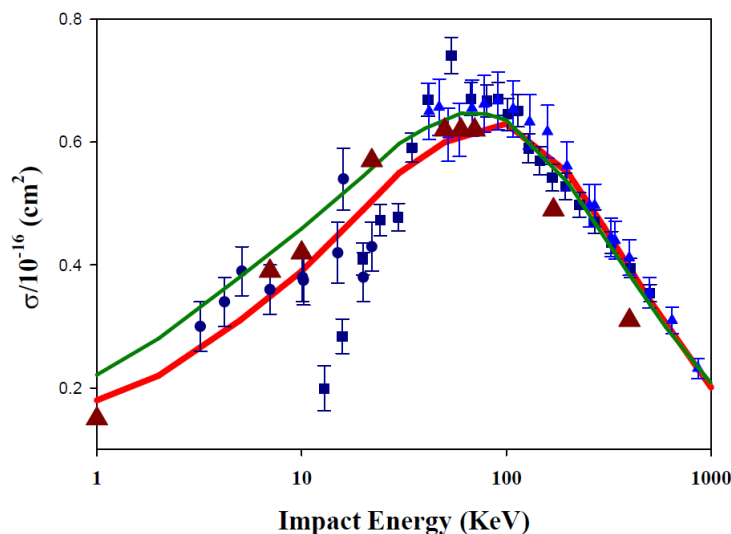
Figure 1. The single-ionization total cross-sections for He atoms in a low-energy antiproton collision. Solid red line: the results of the present coupled channel calculation. Solid green line: cross-sections from [9]. The red triangles are the newest theoretical results from [34]. The blue points are the latest measurements of [3] and the blue triangles and blue squared are the measurements of [2,3], respectively.
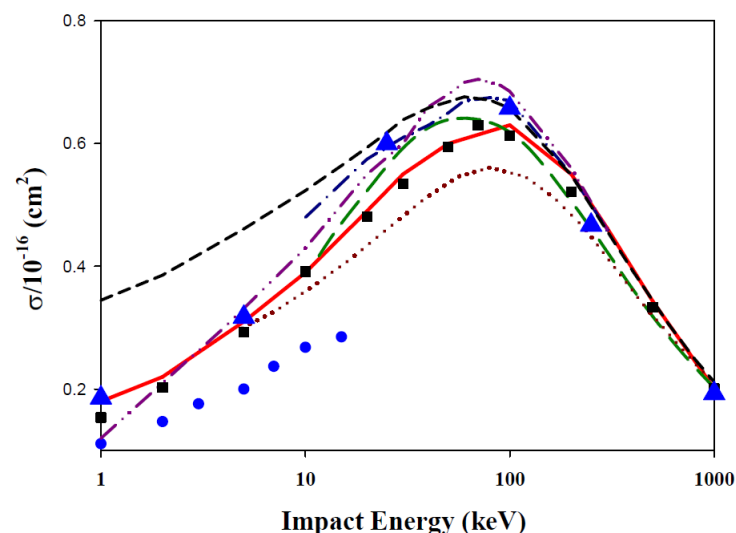

Figure 2. The single-ionization total cross-sections for He atoms in a low-energy antiproton collision. Red solid line: our present coupled channel calculations, whilst the blue points are for Bent et al. [7]; the green long dashed line is for Reading and Ford [6]; the blue dashed-dotted line is for Igarashi et al. [14]; the purple dashed-double-dotted line is for Lee and Tseng [16]; the dark red dotted-line is for Tong et al. [11]; the black dashed line is for Keim et al. [9]; the black squares for Henkel et al. [10]; and the blue triangles are from Schultz [18], respectively.

Figures 3a, 4a and 5a display the DDCS for the single ionization of helium–antiproton impact energies of 10, 50 and 100 keV within the framework of the TDCC method. According to the figures, we can generally conclude the following: In each case, we found a minimum at zero angle indicating the existence of the Coulomb hole ("anti-cusp"). In general, we can say that the anti-cusps always properly appear with the antiproton projectile impact. The projectile energy also enhances the centers of the anti-cusps enhance. At 10 keV, the DDCS are generally smaller than for 50 or 100 keV. Despite numerous theoretical studies investigating the anti-cusp [37,39,41] in recent decades, an experimental observation of the anti-cusp in antiproton impacts is still lacking. Slow electrons are possibly ejected into the backward direction and fast electrons are ejected along the broad ridge identified as the binary encounter (BE) ridge.
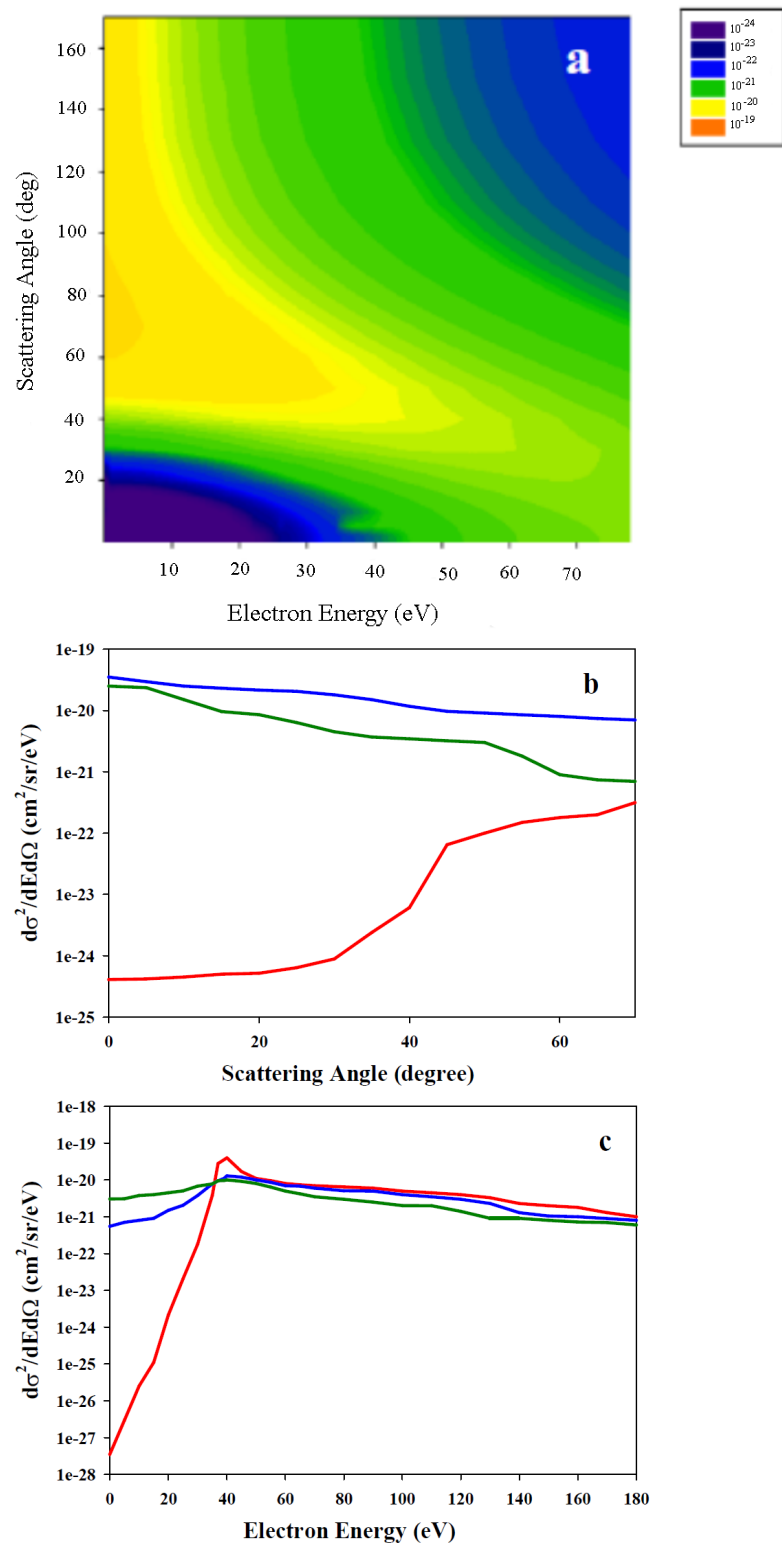
Figure 3. (**a**) Doubly differential electron emission cross-sections emitted from He and 10 keV antiproton impact. (**b**) Three cuts of the DDCS at different angles. The red line is for 0, the blue line is for 60 and the green one is for 120 degrees. (**c**) Three cuts of the DDCS at different energies. The red line is for 20, the blue line is for 40 and the green one is for 60 eV.
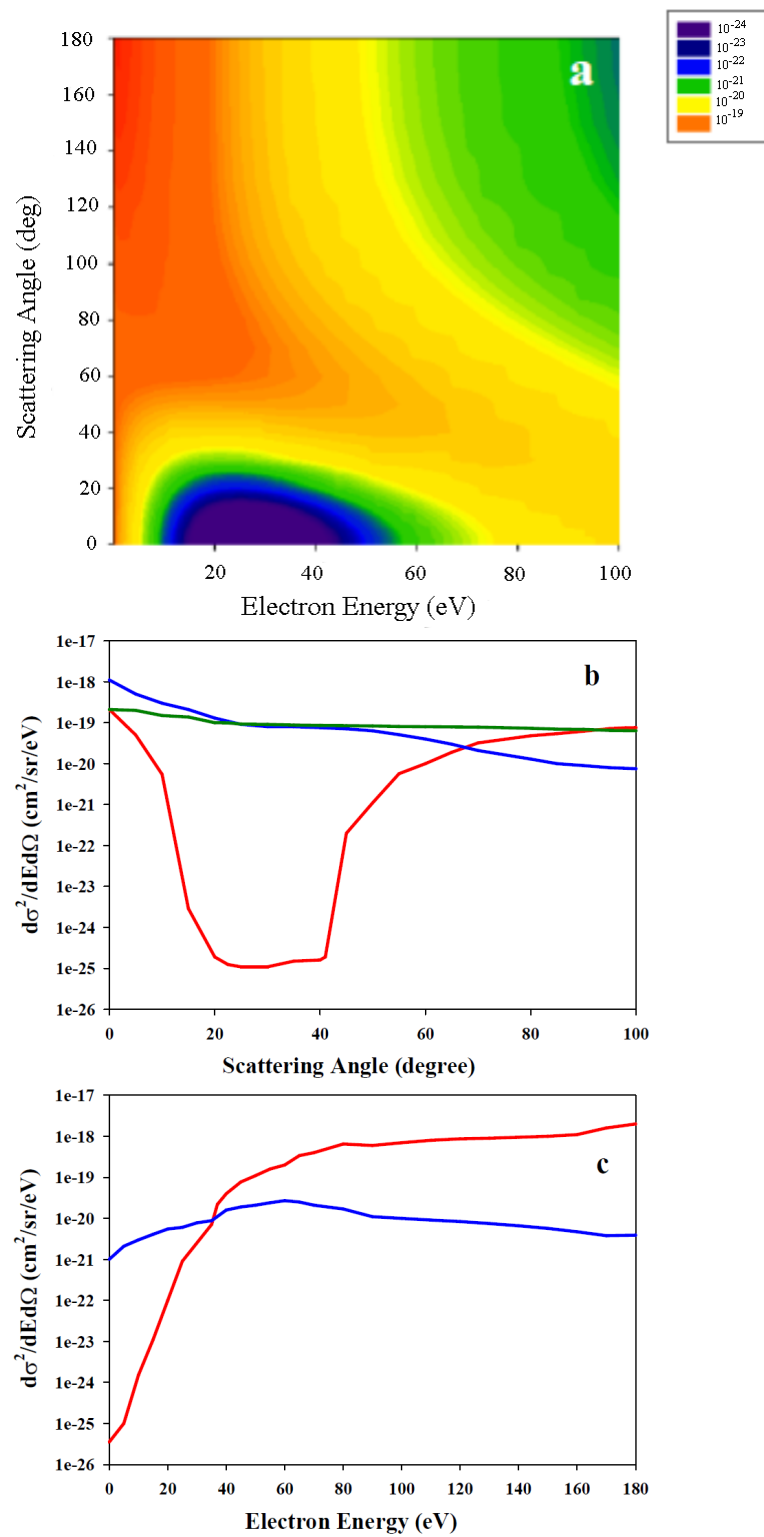
Figure 4. (**a**) The single-ionization total cross-sections for an impact energy of 50 keV. (**b**) Three cuts of the DDCS at different angles. The red line is for 0, the blue line is for 60 and the green one is for 120 degrees. (**c**) Two cuts of the DDCS at different energies. The red line is for 20 and the blue line is for 40 eV.
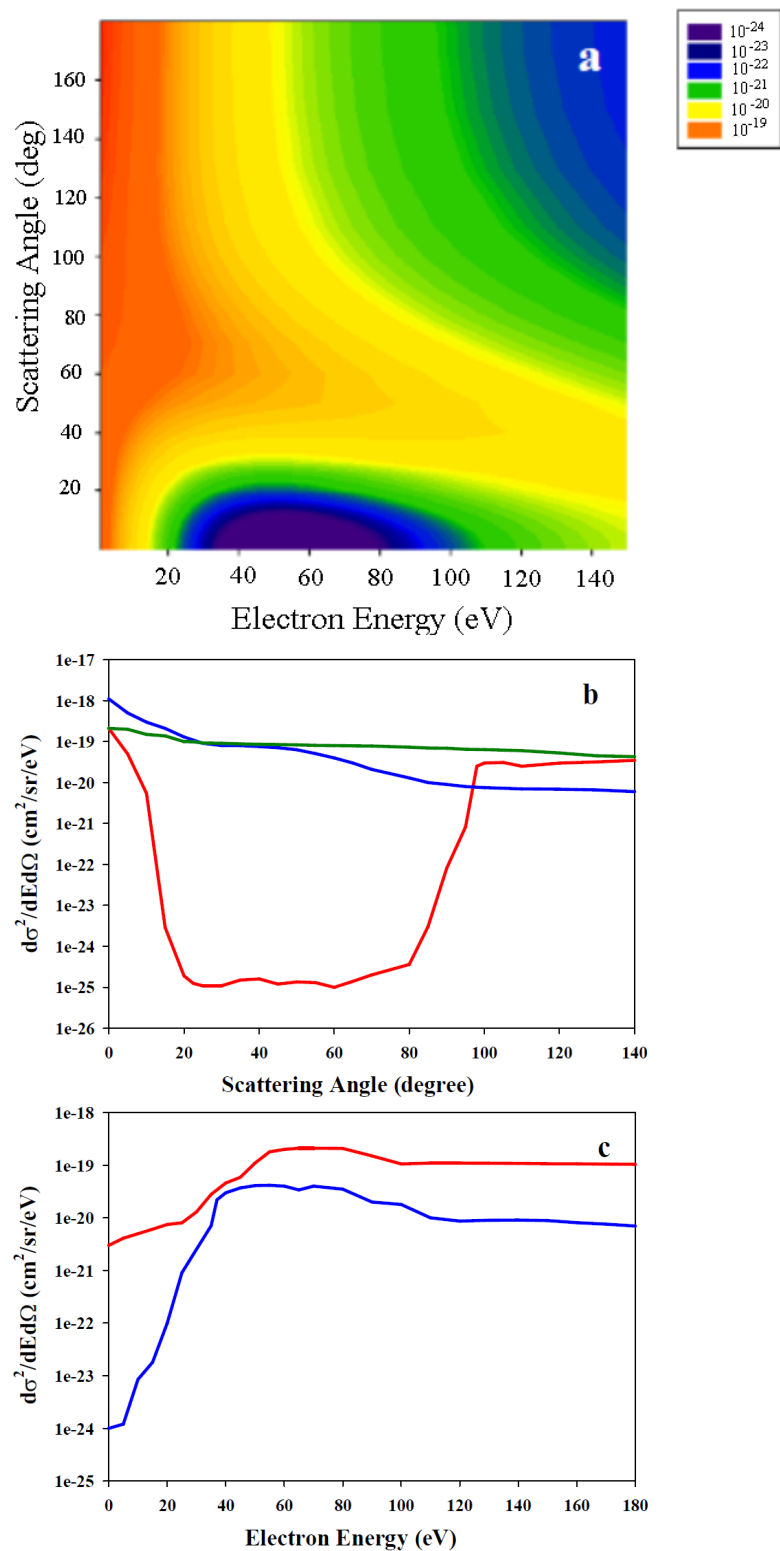
Figure 5. (**a**) T The single-ionization total cross-sections for an impact energy of 100 keV. (**b**) Three cuts of the DDCS at different energies. The red line is for 30, the blue is for 60 and the green one is for 120 degrees. (**c**) Two cuts of the DDCS at different energies. The red line is for 20, the blue line is for 40 eV.

This BE ridge may be the easiest feature to understand as fast electrons are ejected through a series of hard collisions between the projectile and the target known as the

Fermi-shuttle mechanism [53]. For all three energies (10, 50 and 100 keV), the ridge closely follows this trend.

The distribution of slow electrons in backward directions is a clear indication of final-state interactions between the ejected electron and the antiproton. As the force between the electron and the antiproton is repulsive, slow electrons ($v_e < v_p$, where v_e and v_p are the electron and projectile speeds, respectively), lag behind the antiproton and will be scattered to the backward direction. This is the main mechanism which explains the general structure of the collision, therefore the angular distribution in the DDCS will be suppressed in the forward direction, as clearly shown in Figures 3a, 4a and 5a. This is in sharp contrast with the proton impact, where single differential cross-sections will generally peak at small angles and decrease toward large angles. The remarkable contrast with the proton impact is the anti-cusp (void) region for the antiproton impact. This can also be attributed to the repulsive final state interactions.

To have a more transparent overview of the trends of our calculations, we show additional figures, namely cuts at constant energies and cuts at constant scattering angles for all three energies.

Figure 4b shows the energy differential cross-sections at given angles. The cuts are parallel to the x (or energy) axis at 0, 60 and 120 degrees which are at the cusp, at the ridge and above the ridge. The presence of the anti-cusp is evident. At low-electron energies (around the ionization threshold), the cross-sections are 10,000 times lower for 20 degree emission angle than for the 60 degree emission angle. Note that a factor of 100 remains even at 70 eV electron energies. The ratio of the cross-sections between 60 and 120 degrees are much smaller.

Figure 3c shows the angular differential cross-sections at 20, 40 and 60 eV energies. We note that at zero scattering angle the electrons with 20 eV kinetic energy have a 10,000 times smaller cross-section than the electrons with energy of 40 eV.

Figure 5a shows the DDCS for a 50 keV antiproton impact energy. The general features remain the same—however, all differential cross-sections are larger in accordance with the total cross-sections. The position of the anti-cusp lies at 30 eV. On the contrary, the maximal widths of the corresponding anti-cusp angle is reduced from 20 to 5 degrees. Figure 5b shows the cross-sections at different emission angles. Note that the cross-sections lie in almost the same magnitude in all directions. This is drastically different to the 10 keV energy case. Figure 5c shows the angular distributions for 20 and 40 eV energy electrons. Here again, at a zero scattering angle, the electrons with 20 eV kinetic energy have 10,000-fold smaller cross-sections than the electrons with an energy of 40 eV.

Figure 5 shows the ionization cross-sections for 100 keV antiproton with the same general features. The center of the anti-cusp is at 50 eV with the energy widths of ± 30 eVs. It is clear to see in Figure 5b that, at an emission angle of zero and at back scattering, all three cross-sections lie in almost the same magnitude. Figure 5c shows a significant difference to Figures 3c and 4c in that the cross-section curves do not cross—a clear fingerprint that the whole distribution has become much more flat.

4. Summary and Conclusions

The total, singly and doubly differential ionization cross-sections for antiproton–helium atom collisions at impact energies of 10, 50 and 100 keV were presented. The calculations were based on an ab initio time-dependent coupled channel method using a finite basis set of regular helium Coulomb wave packets and Slater function. A semi classical approximation was applied with the time-dependent Coulomb potential to describe the antiproton–electron interaction. We found a strong final state interaction between the antiprotons and the ejected electrons in the forward scattering angles. We clearly identified the existence of the formation of an anti-cusp for each antiproton impact. We hope that our recent calculations will further encourage experimentalists to carry out differential cross-section measurements in the near future.

References

1. International Workshop on Atomic Collisions and Atomic Spectroscopy with Slow Antiproton, Book of Abstracts Tsurumi, Yokohama, Kanagawa, Japan. Available online: http://radphys4.c.u-tokyo.ac.jp/pbar99/AbstractFinal3.pdf (accessed on 22 August 1999).
2. Andersen, L.H.; Hvelplund, P.; Knudsen, H.; Moller, S.P.; Pedersen, J.O.P.; Tang-Petersen S.; Uggerhoj E.; Elsner, E.K.; Morenzoni, E. Single ionization of helium by 40-3000-keV antiprotons. *Phys. Rev. A* **1990**, 40, 7366. [CrossRef] [PubMed]
3. Hvelplund, P.; Knudsen, H.; Mikkelsen, H.U.; Morenzoni, E.; Moller, S.P.; Uggerhoj, E.; Worm, T. Ionization of helium and molecular hydrogen by slow antiprotons. *J. Phys. B* **1994**, *27*, 925. [CrossRef]
4. Knudsen, H.; Kristiansen, H.-P. E.; Thomsen, H.D.; Uggerhoj, U.I.; Ichioka, T.; Moller, S.P.; Hunniford, C.A.; Mullough, R.W.; Charlton, W.; Kuroda, M.N.; et al. Target Structure Induced Suppression of the Ionization Cross Section for Very Low Energy Antiproton-Hydrogen Collisions. *Phys. Rev. Lett.* **2008**, *101*, 043201. [CrossRef] [PubMed]
5. Ford, A.L.; Reading, J.F. Improved forced impulse method calculations of single and double ionization of helium by collision with high-energy protons and antiprotons. *J. Phys. B At. Mol. Opt. Phys.* **1994**, *30*, 4215. [CrossRef]
6. Reading, J.K.; Bronk, T.; Ford, A.L.; Wherman, L.; Hall, K.A. Multi-cut forced impulse method single-ionization cross sections for slow antiprotons on helium. *J. Phys. B* **1997**, *30*, L189. [CrossRef]
7. Bent, G.; Krstic, P.S.; Schultz, D.R. The multielectron, hidden crossings method for inelastic processes in slow ion/atom–atom collisions. *J. Chem. Phys.* **1998**, *108*, 1459. [CrossRef]
8. Lüdde, H.J.; Kirchner, T.; Horbatsch, M. Quantum Mechanical Treatment of Ion Collisions with Many-Electron Atoms. In *Photonic, Electronic, and Atomic Collisions*; Burgdörfer, J., Ed.; Rinton Press: Princeton, UK, 2020; p. 708.
9. Keim, M.; Achenbach, A.; Lüdde, H.J.; Kirchner, T. Microscopic response effects in collisions of antiprotons with helium atoms and lithium ions. *Phys. Rev. A* **2003**, *67*, 062711. [CrossRef]
10. Henkel, N.; Keim, M.; Lüdde, H.J.; Kirchner, T. Density functional theory investigation of antiproton-helium collisions. *Phys. Rev. A* **2003**, *80*, 032704. [CrossRef]
11. Tong, X.-M.; Watanabe, T.; Kato, D.; Ohtani, S. Ionization of atomic hydrogen by antiproton impact: A direct solution of the time-dependent Schrödinger equation. *Phys. Rev. A* **2002**, *66*, 032709. [CrossRef]
12. Schiwietz, G.; Willie, U.; Muino, R.D.; Fainstein, P.D.; Grande, P.L. Comprehensive analysis of the stopping power of antiprotons and negative muons in He and H 2 gas targets. *J. Phys. B* **1996**, *29*, 307. [CrossRef]
13. Wherman, L.A.; Ford, A.L.; Reading, J.F. Double ionization of helium by slow antiprotons. *J. Phys. B* **1996**, *29*, 5831. [CrossRef]
14. Igarashi, A.; Ohsaki, A.; Nakazaki, S. Single ionization of helium by antiproton impact. *Phys. Rev. A* **2000**, *62*, 052722. [CrossRef]
15. Díaz, C.; Martin, F.; Salin. A. Time-dependent close-coupling calculations of double ionization of helium by protons and antiprotons. *J. Phys. B* **2002**, *35*, 2555. [CrossRef]
16. Lee, T.G.; Tseng, H.C.; Lin, C.D. Evaluation of antiproton-impact ionization of He atoms below 40 keV. *Phys. Rev. A* **2000**, *61*, 062713. [CrossRef]
17. Pindzola, M.S.; Lee, T.G.; Colgan, J. Antiproton-impact ionization of H, He and Li. *J. Phys. B. At. Mol. Opt. Phys.* **2011**, *44*, 205204. [CrossRef]
18. Schulz, D.R.; Krstic, P.S. Ionization of helium by antiprotons: Fully correlated, four-dimensional lattice approach. *Phys. Rev. A* **2003**, *67*, 022712. [CrossRef]
19. Sahoo, S.; Mukherjee, S.C.; Walters, H.R.J. Ionization of atomic hydrogen and He+ by slow antiprotons. *J. Phys. B* **2004**, *37*, 3227. [CrossRef]
20. Martin, F. Ionization and dissociation using B-splines: Photoionization of the hydrogen molecule. *J. Phys. B* **1997**, *32*, R197. [CrossRef]
21. Foster, M.; Colgan, J.; Pindzola, M.S. Fully Correlated Electronic Dynamics for Antiproton Impact Ionization of Helium. *Phys. Rev. Lett.* **2008**, *100*, 033201. [CrossRef]
22. Fainstein, P.D.; Ponce, V.H.; Rivarola, R.D. Z3P effects in the ionization of helium by ion impact. *Phys. Rev. A* **1987**, *36*, 3639. [CrossRef]
23. Schultz, D.R. Comparison of single-electron removal processes in collisions of electrons, positrons, protons, and antiprotons with hydrogen and helium. *Phys. Rev. A* **1989**, *40*, 2330. [CrossRef] [PubMed]
24. Barna, I.F.; Gulyás, L.; Tőkési, K.; Burgdörfer, J. Total and angular differential cross sections of electrons emitted in collision between antiprotons and helium atoms. *Rad. Phys. Chem.* **2007**, *76*, 495. [CrossRef]

25. Tőkési, K.; Wang, J.; Gulyás, L.; Burgdörfer, J. Angular and energy differential electron emission cross sections in collisions between antiprotons and helium atoms. *Hyperfine Interact.* **2009**, *194*, 45. [CrossRef]
26. Kirchner, T.; Knudsen, H. Current status of antiproton impact ionization of atoms and molecules: Theoretical and experimental perspectives. *J. Phys. B* **2011**, *44*, 122001. [CrossRef]
27. Baxter, M.; Kirchner, T. Correlation in time-dependent density-functional-theory studies of antiproton-helium collisions. *Phys. Rev. A* **2013**, *87*, 062507. [CrossRef]
28. Pindzola, M.S.; Lee, T.G.; Colgan, J. Antiproton-impact ionization of H2 at low incident energies. *J. Phys. B. At. Mol. Opt. Phy.* **2014**, *47*, 185202. [CrossRef]
29. Borbély, S.; Tong, X.-M.; Nagele, S.; Feist, J.; Bøezinová, I.; Lackner, F.; Nagy, L.; Tőkési, K.; Burgdörfer, J. Electron correlations in the antiproton energy-loss distribution in He. *Phys. Rev. A* **2014**, *98*, 012707. [CrossRef]
30. Abdurakhmanov, I.B.; Kadyrov, A.S.; Bray, I.; Bartschat, K. Wave-packet continuum-discretization approach to single ionization of helium by antiprotons and energetic protons. *Phys. Rev. A* **2017**, *96*, 022702. [CrossRef]
31. Jonsell, S. Collisions involving antiprotons and antihydrogen: An overview. *Phil. Trans. R. Soc. A* **2018**, *376*, 20170271. [CrossRef]
32. Gao, J.W.; Miteva, T.; Wu, Z.; Wang, J.G.; Dubois, A.; Sisourat, N. Single- and double-ionization processes using Gaussian-type orbitals: Benchmark on antiproton-helium collisions in the keV-energy range. *Phys. Rev. A* **2021**, *103*, L030803. [CrossRef]
33. Lüdde, H.J.; Horbatsch, M.; Kirchner, T. Calculation of energy loss in antiproton collisions with many-electron systems using Ehrenfest's theorem. *Phys. Rev. A* **2021**, *104*, 032813. [CrossRef]
34. Jia, C.C.; Kirchner, T.; Gao, J.W.; Wu, Y.; Wang, J.G.; Sisourat, N. Single- and double-ionization processes of antiproton-helium and antiproton–molecular hydrogen collisions in the keV energy range. *Phys. Rev. A* **2023**, *107*, 012808. [CrossRef]
35. Crooks, G.B.; Rudd, M.E. Experimental Evidence for the Mechanism of Charge Transfer into Continuum States. *Phys. Rev. Lett.* **1970**, *25*, 1599. [CrossRef]
36. Stolterfoht, N.; DuBois, R.D.; Rivarola, R.D. *Electron Emission in Heavy Ion-Atom Collisions*; Springer: Berlin, Germany, 1997.
37. Reinhold, C.O.; Burgdörfer, J. The classical limit of ionization in fast ion-atom collisions. *J. Phys. B* **1993**, *26*, 3101. [CrossRef]
38. Yamazuki, Y.; Kuroki, K.; Komaki, K.; Andersen, L.H.; Horsdal-Pettersen, E.; Hvelplund, P.; Knudsen, H.; Moller, S.P.; Uggerhoj, E.; Elsner, K. Measurements of Electron Spectra in the Forward Direction in Slow-Antiproton Carbon-Foil Collisions. *J. Phys. Soc. Jpn.* **1990**, *59*, 2643. [CrossRef]
39. Burgdörfer, J.; Wang, J.; Müller, J. Forward electron production in antimatter-solid collisions. *Phys. Rev. Lett.* **1989**, *62*, 1599. [CrossRef]
40. Fainstein, P.D.; Ponce, V.H.; Rivarola, R.D. Ionisation of helium by antiproton and proton impact. *J. Phys. B* **1989**, *21*, 2989. [CrossRef]
41. Olson, R.E.; Gay, T.J. Dynamics of Antimatter-Atom Collisions. *Phys. Rev. Lett.* **1988**, *61*, 302. [CrossRef]
42. Reinhold, C.O.; Olson, R.E. Classical two-center effects in ejected-electron spectra from p+, p−, and He2++He collisions at intermediate energies. *Phys. Rev. A* **1989**, *39*, 3861. [CrossRef]
43. Barna, I.F.; Grün, N.; Scheid, W. Coupled-channel study with Coulomb wave packets for ionization of helium in heavy ion collisions. *Eur. Phys. J. D* **2003**, *25*, 239. [CrossRef]
44. Barna, I.F. Ionization of Helium in Relativistic Heavy-Ion Collisions. Doctoral Thesis, University Gießen, Giessen, Germany, 2002.
45. Barna, I.F. Ionization of helium in positron collisions. *Eur. Phys. J. D* **2004**, *30*, 5. [CrossRef]
46. Barna, I.F.; Rost, J.M. Photoionization of helium with ultrashort XUV laser pulses. *Eur. Phys. J. D* **2003**, *27*, 287. [CrossRef]
47. Barna, I.F.; Tőkési, K.; Burgdörfer, J. Single and double ionization of helium in heavy-ion impact. *J. Phys. B* **2005**, *38*, 1001. [CrossRef]
48. Pocsai, M.A.; Barna, I.F.; Tőkési, K. Photoionisation of rubidium in strong laser fields. *Eur. Phys. J. D* **2019**, *73*, 74. [CrossRef]
49. Landau, L.D.; Lifshitz, E.M. *Mechanics*; Pergamon Press: Oxford, UK, 1960; Chapter 19, p. 53.
50. Frank, W.; Olver, J.; Daniel, W.; Lozier, W.; Boisvert, R.F.; Clark, C.W. *NIST Handbook of Mathematical Functions*; Cambridge University Press: Cambridge, UK, 2010.
51. Ho, Y.K. Positron annihilation in positronium hydrides. *Phys. Rev. A* **1986**, *34*, 4402. [CrossRef]
52. Maruhn, J.A.; Reinhard, P.-G.; Suraud, E. *Simple Models of Many–Fermion Systems*; Springer: Berlin/Heidelberg, Germany, 2010; Appendix A5.1, p. 260.
53. Sulik, B.; Koncz, C.S.; Tőkési, K.; A. Orbán, A.; Berényi, D. Evidence for Fermi–Shuttle Ionization in Intermediate Velocity C++Xe Collisions. *Phys. Rev. Lett.* **2002**, *88*, 073201. [CrossRef] [PubMed]